



Artery Research

ISSN (Online): 1876-4401

ISSN (Print): 1872-9312

Journal Home Page: <https://www.atlantis-press.com/journals/artres>

Detection of aortic wall inclusions using regional pulse wave propagation and velocity *in silico*

Danial Shahmirzadi, Elisa E. Konofagou

To cite this article: Danial Shahmirzadi, Elisa E. Konofagou (2012) Detection of aortic wall inclusions using regional pulse wave propagation and velocity *in silico*, Artery Research 6:3, 114–123, DOI: <https://doi.org/10.1016/j.artres.2012.05.004>

To link to this article: <https://doi.org/10.1016/j.artres.2012.05.004>

Published online: 3 December 2019



Detection of aortic wall inclusions using regional pulse wave propagation and velocity *in silico*

Danial Shahmirzadi, Elisa E. Konofagou*

Ultrasound and Elasticity Imaging Laboratory, Department of Biomedical Engineering, Columbia University, New York, NY 10027, USA

Received 10 March 2012; received in revised form 10 May 2012; accepted 24 May 2012
Available online 17 July 2012

KEYWORDS

Aortic pulse wave velocity (PWV);
Aortic wall stiffness;
Regional stiffening;
Regional softening;
Pulse wave imaging (PWI)

Abstract Monitoring of the regional stiffening of the arterial wall may prove important in the diagnosis of various vascular pathologies. The pulse wave velocity (PWV) along the aortic wall has been shown to be dependent on the wall stiffness and has played a fundamental role in a range of diagnostic methods. Conventional clinical methods entail global examination of the pulse traveling between two remote sites, e.g. femoral and carotid arteries, to provide an average PWV estimate. However, the majority of vascular diseases entail regional vascular changes and therefore may not be detected by a global PWV estimate. In this paper, a fluid-structure interaction study of straight-geometry aortas of 350 mm length is described aimed at examining the effects of regional stiffness changes on the PWV. Five homogeneous aortas with increasing wall stiffness as well as two aortas with soft and hard inclusions of 5 mm length were considered. In each case, spatio-temporal maps of the wall motion were used to analyze the regional pulse wave propagation. On the homogeneous aortas, increasing PWVs were found to increase with the wall moduli ($R^2=0.9988$), indicating the reliability of the model to accurately represent the wave propagation. On the inhomogeneous aortas, formation of reflected and standing waves was observed at the site of the hard and soft inclusions, respectively. Neither the hard nor the soft inclusion had a significant effect on the velocity of the traveling pulse beyond the inclusion site, which supported the hypothesis that a global measurement of the average PWV could fail to detect small, regional abnormalities.

© 2012 Association for Research into Arterial Structure and Physiology. Published by Elsevier B.V. All rights reserved.

Introduction

Changes in the vascular mechanical properties may have immediate ramifications on the onset and progression of

cardiovascular diseases (CVD) such as the increase of the systolic blood pressure due to arterial wall stiffening.¹ Increase in the aortic stiffness has been reported in different studies as an independent indicator of all-cause

* Corresponding author. Tel.: +1 212 342 0863; fax: +1 212 342 1648.
E-mail address: ek2191@columbia.edu (E.E. Konofagou).

and CVD-related mortalities such as those related to primary coronary events and fatal stroke in hypertensive patients,^{2,3} cardiovascular risks related to diabetes,^{4,5} vascular calcification^{6,7} and aortic aneurysms (for which both wall stiffening and softening have been reported).^{8–14} Collectively, there has been a consensus that assessing arterial stiffness should be part of the routine clinical diagnosis, treatment and follow-up procedures.^{15,16}

Methods for measuring arterial stiffness typically fall into two broad categories. The first set of methods includes those based on radial pulsation such as diameter-pressure measurements. A major drawback in using these methods is the requirement for the central pressure measurement, which is either invasive, e.g., through catheterization¹⁷ or incurs large degrees of inaccuracy using empirical transfer functions of peripheral pressure data, e.g., tonometry.¹⁸ The next set of methods includes those based on measuring the velocity of the longitudinal aortic pulse wave. The pulse wave velocity (PWV) has been shown to be related to the underlying tissue stiffness through the Moens–Korteweg equation^{19,20} and has been used in a variety of applications.^{21–23} The quantitative stiffness measurements based on the Moens–Korteweg relationship could be inaccurate in applications—such as the present study—where certain underlying assumptions, e.g. infinitely long and thin-walled cylinder, are not met.^{17,23} However, the qualitative relationship between stiffness and PWV remains valid and forms the basis of the PWI method for detection of regional changes in stiffness based on the PWV measurements.

Different methods have been proposed for the noninvasive estimation of PWV.^{24,25} The current gold standard in clinical practice is to obtain the global PWV by measuring the temporal pulse pressure profiles at two remote sites, typically the carotid and femoral arteries.^{16,26} The time delay between the two ECG-synchronized waveforms (Δt) is estimated²⁷ and divided by the distance (D) between the two sites, obtained by over-the-skin measurements, in order to estimate the global PWV through $PWV = D/\Delta t$. Such methods are at the core of most clinical studies involving the measurement of arterial stiffness.^{28–30} However, there are drawbacks associated with the global PWV measurement which can largely impair the accuracy of the method. For instance, the lack of knowledge of the exact arterial geometry as well as the assumption of a single longitudinal flow direction between the carotid and the femoral arteries may lead to erroneous estimation of the true distance.³¹ More importantly, the wall stiffness and PWV have been shown to vary locally along the arterial wall.^{17,32} Therefore, the use of a global PWV may not detect the early onset or focal disease such as an aneurysm.^{32–34} These and other fundamental limitations of these methods have been reviewed in detail elsewhere.³⁵

Imaging modalities such as ultrasound^{36–45} and MRI^{46–50} have been used for noninvasive imaging of the arterial wall at multiple time-points during the cardiac cycle in order to track the propagation of the transient vibrations along the arterial wall in 2D and estimate the PWV; in some cases, along with simultaneous pressure measurements for measuring parameters such as the augmentation index. More recently, the ultrasound-based method of Pulse Wave

Imaging (PWI) has been developed to fully map and analyze the wave propagation with high temporal and spatial resolutions and to measure the local PWV. The PWI method has been applied in normal and aneurysmal mouse aortas *in vivo*^{14,51} as well as normal and aneurysmal human aortas,^{52–54} aneurysmal and hypertensive subjects,⁵⁵ and experimental phantoms,³¹ and has also been compared against applanation tonometry in humans.⁵⁶ However, the reliability of PWI in estimating regional PWV needs to be verified in the presence of discontinuities at the sites of regional change in wall composition and geometry such as arterial branches and aneurysmal lesions to better determine its clinical potential.

Modeling of the aortic pulsation can therefore provide additional insight into the pulse wave characteristics in arteries with irregular geometry and abnormal wall properties, and the results can be used as a guideline for *in vivo* animal and clinical examinations. Finite-element methods (FEM) used to model cardiovascular biomechanics primarily rely on solid-state (SS) modeling of blood vessels experiencing static or pulsatile internal pressure replicating the hemodynamic effects.^{57,58} More recently, fully-coupled fluid-structure interaction (FSI) simulations using patient-specific geometries and anisotropic finite-strain constitutive relations have been reported in healthy and diseased arteries,^{57,59–62} aiming at computing parameters such as fluid velocity and pressure as well as wall strain and stress.^{63,64} Scotti et al. have extracted temporal information on the arterial wall displacement during dynamic FSI; however, no spatial information was obtained and thus no PWV measurements could be performed.⁶⁵ Preliminary studies on developing finite-element models of aortic pulse wave propagation have been reported by our group.⁶⁶ In particular, applying Coupled Eulerian-Lagrangian (CEL) analysis for simulation of arterial pulse wave propagation has previously been validated against phantom and *in vitro* canine studies.^{67–69}

In this paper, we develop a fully dynamic FSI model of a traveling pulse wave in straight-geometry aortas of homogenous and inhomogeneous (inclusion) models in order to obtain the regional PWV estimates. Spatio-temporal maps of the wall motion will be used to calculate the regional PWVs on the homogenous and on the inclusion models to better understand the effects of focal changes on the regional and global PWVs.

Methods

Numerical modeling

A full 3D dynamic FSI model of pulse wave propagation was constructed in Coupled Eulerian-Lagrangian (CEL) explicit solver of Abaqus 6.10-1 (*Simulia, RI, USA*). A workstation with Intel® Xeon® CPU @2.33 GHz and 32 GB RAM was used to perform the computations. The aortic wall was modeled as a purely elastic material: Young's modulus of $E = 2.56\text{--}7.68$ MPa, density $\rho_s = 1050$ kg/m³, Poisson's ratio $\nu = 0.48$.^{65,70,71} In order to follow the configurations used in our previously reported phantom and *in vitro* studies,^{54,67–69} fluid was assumed to be Newtonian, with material properties as follows: density $\rho_f = 1000$ kg/m³,

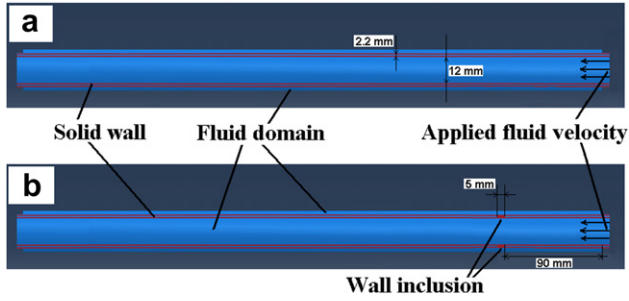


Figure 1 Longitudinal cross-section of the aorta-fluid geometry in Abaqus: (a) Homogenous model, (b) Inclusion model.

reference sound speed $c_0 = 1483 \text{ m/s}$ and viscosity $\eta = 0.0001 \text{ Ns/m}^2$.^{72,73} The Lagrangian part was constructed as a straight cylindrical geometry ($r_i = 12 \text{ mm}$; $t = 2.2 \text{ mm}$), encompassed by the Eulerian domain simulating the presence of a fluid medium. A total of seven modeling parameters were considered: five with homogeneous walls of distinct stiffness (Fig. 1a) and two with inhomogeneous walls containing hard or soft inclusions (Fig. 1b), respectively. The normal homogenous model was assumed to have a Young's modulus equal to $E_1 = 2.56 \text{ MPa}$.¹⁰ To simulate early onset of diseases such as atherosclerosis or aneurysm,^{7,10} four other homogenous models were constructed with Young's moduli of $E_2 = 1.5E_1 = 3.84 \text{ MPa}$, $E_3 = 2E_1 = 5.12 \text{ MPa}$, $E_4 = 2.5E_1 = 6.40 \text{ MPa}$ and $E_5 = 3E_1 = 7.68 \text{ MPa}$, respectively. For the models with an inclusion, the same geometry was used but with an inclusion of axial length 5 mm , located at 90 mm from vessel inlet (Fig. 1b). A Young's modulus of $E_{hard-incl} = 7.68 \text{ MPa}$ and $E_{soft-incl} = 2.56 \text{ MPa}$ was used to represent the hard and soft inclusions on the $E_1 = 2.56 \text{ MPa}$ and $E_5 = 7.68 \text{ MPa}$ models, respectively. In all models, both the inlet and outlet were fully constrained in x-y-z dimensions. A rectangular function with magnitude $V_0 = 5 \text{ m/s}$ was set as the initial velocity on the tube inlet which served as the driving force at the FSI and caused the dynamic wall motion. A frictionless fluid-structure interface was defined between the wall and the medium. Both the Eulerian and Lagrangian domains were meshed using same-size linear hexagonal 3D elements to increase the FSI mesh consistency. A mesh

seeding topology was designed to generate a minimum of three layers of elements across the wall thickness and a seeding size of 4 mm was found to be optimal in providing a converging solution while computationally affordable. The model contained a total number of 17688 elements and 21780 nodes. The initial time increment was $9.57E-07 \text{ s}$ where the average stable time increment changed between $2.70E-06$ and $4.29E-06 \text{ s}$ across the 7 models. The radial displacement of the entire wall along the tube (axial spatial resolution of 5 mm) was measured on multiple time-points (temporal resolution of 0.375 ms) (Fig. 2) and the information was mapped onto a 2D spatio-temporal plane which allowed the visualization of the entire wave propagation and tracking of the wave peak. Unlike in the experimental phantom and *in vivo* studies where the wave foot has been reported to be more robust for tracking the wave than the peak,^{51,55} in the current simulations, the wave peak was found to be as robust and a better marker for tracking the traveling wave. The PWV was calculated as the slope of the linear regression fit to the wave peak locations versus time.

PWV-based regional stiffness detection

The spatio-temporal maps were used to analyze the pulse wave propagation both qualitatively (e.g. detecting different forward and reflected waves) and quantitatively (e.g. computing the PWV on each wave). Both qualitative and quantitative measures were used to monitor the wall stiffness and its regional changes. The PWV can be used to estimate the Young's modulus, E , via the modified Moens–Korteweg equation^{17,19,20}:

$$E = \frac{1}{t} 2(1 - \nu^2) \cdot \rho \cdot r \cdot PWV^2 \quad (1)$$

where ν , t and r denote the wall Poisson's ratio, thickness and radius, respectively, and ρ is the wall density. As mentioned earlier, due to the violation of the underlying assumptions discussed elsewhere,^{17,23,69} the Moens–Korteweg relationship was used here to merely identify the relative change in stiffness based on changes in the PWV. Given that the same Poisson's ratio, wall density and geometry were assumed for all different models used in this study, Eq. (1) can be rewritten in the following form:

$$\frac{E}{E'} = \left(\frac{PWV}{PWV'} \right)^2 \quad (2)$$

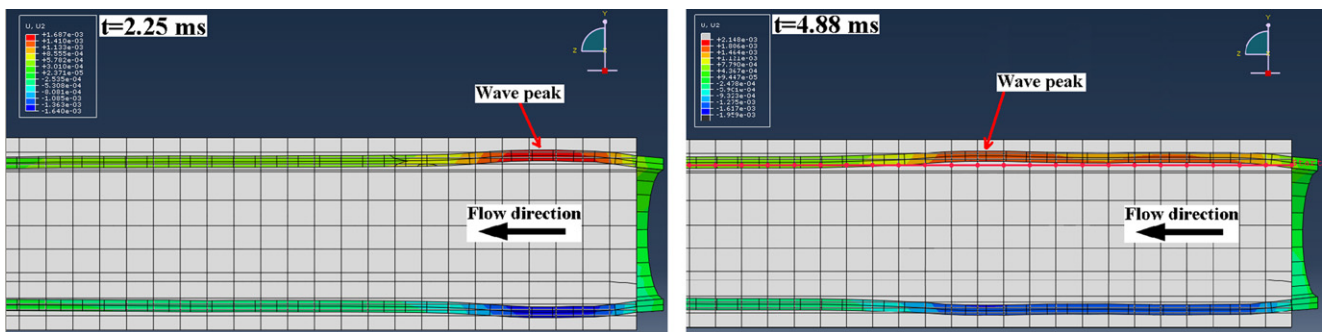


Figure 2 Examples of two temporal frames of the pulse-wave-induced wall displacement in the homogenous model showing the forward traveling wave.

where PWV and PWV' are the pulse wave velocities associated with two different wall moduli of E and E' , respectively. This equation indicates that a linear correlation exists between the Young's modulus and the pulse wave velocity-squared.

Results

Homogenous walls

Figs. 3–5 illustrate the 3D waterfall plots as well as the corresponding 2D spatio-temporal maps of the wall motion, obtained from the three homogenous models with Young's modulus of $E_1 = 2.56 \text{ MPa}$, $E_3 = 5.12 \text{ MPa}$ and $E_5 = 7.68 \text{ MPa}$, respectively, showing the PWV to increase with the wall stiffness. For all five homogenous models, the linear regression fit to the wave peaks yields the following velocities: $PWV_1 = 12.59 \text{ m/s}$ ($R^2 = 0.9981$), $PWV_2 = 15.25 \text{ m/s}$ ($R^2 = 0.9983$), $PWV_3 = 17.45 \text{ m/s}$ ($R^2 = 0.9991$), $PWV_4 = 19.15 \text{ m/s}$ ($R^2 = 0.9986$) and $PWV_5 = 20.81 \text{ m/s}$ ($R^2 = 0.9988$) on the models with modulus E_1 through E_5 , respectively.

PWV-E correlation

Fig. 6 shows the pulse wave velocity-squared versus Young's modulus data from the five aforementioned homogenous

models. A very high correlation was established ($R^2 = 0.9988$) which indicates that the current model is able to accurately detect the increase in the wall modulus based on the higher pulse wave velocity.

Wall with hard inclusion

The 3D waterfall plots as well as the 2D spatio-temporal maps of the wall motion obtained from the model with hard inclusion are shown in Fig. 7. Qualitative examination of the plots shows that a portion of the supra-inclusion forward wave continues to travel through the inclusion, while another portion of it gets reflected at the inclusion site. However, the hard inclusion does not seem to affect the velocity of the forward wave beyond the inclusion site. The quantitative pulse wave velocity measurements obtained from the linear fits indicate the supra- and infra-inclusion PWVs as 12.24 m/s ($R^2 = 0.9970$) and 12.59 m/s ($R^2 = 0.9951$), respectively. A PWV of 7.61 m/s ($R^2 = 0.9516$) was measured on the reflected wave.

Wall with soft inclusion

Similarly in the case of the soft inclusion model, the 3D waterfall plots as well as the 2D spatio-temporal maps of the wall motion are shown in Fig. 8. As expected, the highest wall

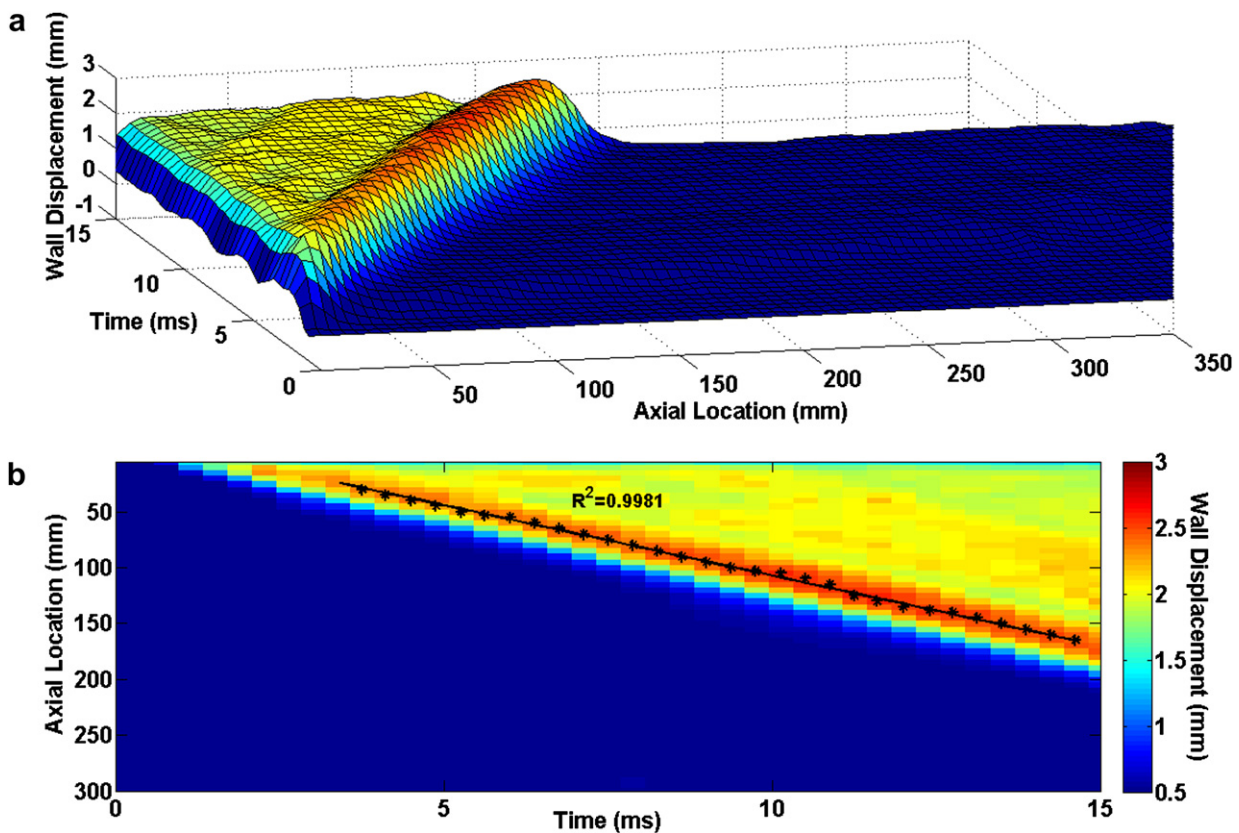


Figure 3 Homogenous model with Young's modulus of $E_1 = 2.56 \text{ MPa}$: (a) Waterfall plots of the wall displacement against temporal and spatial coordinates on the aortic wall. (b) 2D spatio-temporal plot of the wall displacement. Also shown are the peaks (black asterisks) on the forward wave and the regression fit (black line).

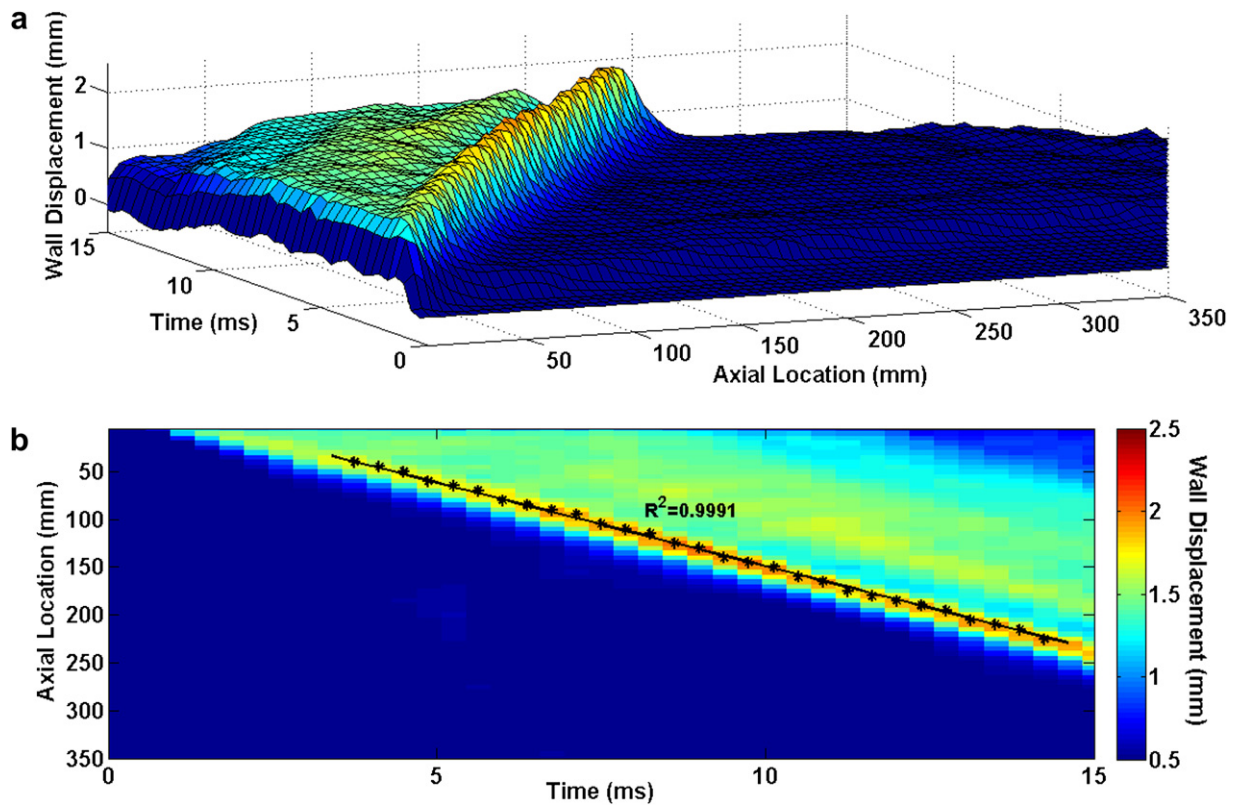


Figure 4 Homogenous model with Young's modulus of $E_3 = 5.12 \text{ MPa}$: (a) 3D waterfall plots of the wall displacement against temporal and spatial coordinates on the aortic wall. (b) 2D spatio-temporal plot of the wall displacement. Also shown are the peaks on the forward wave.

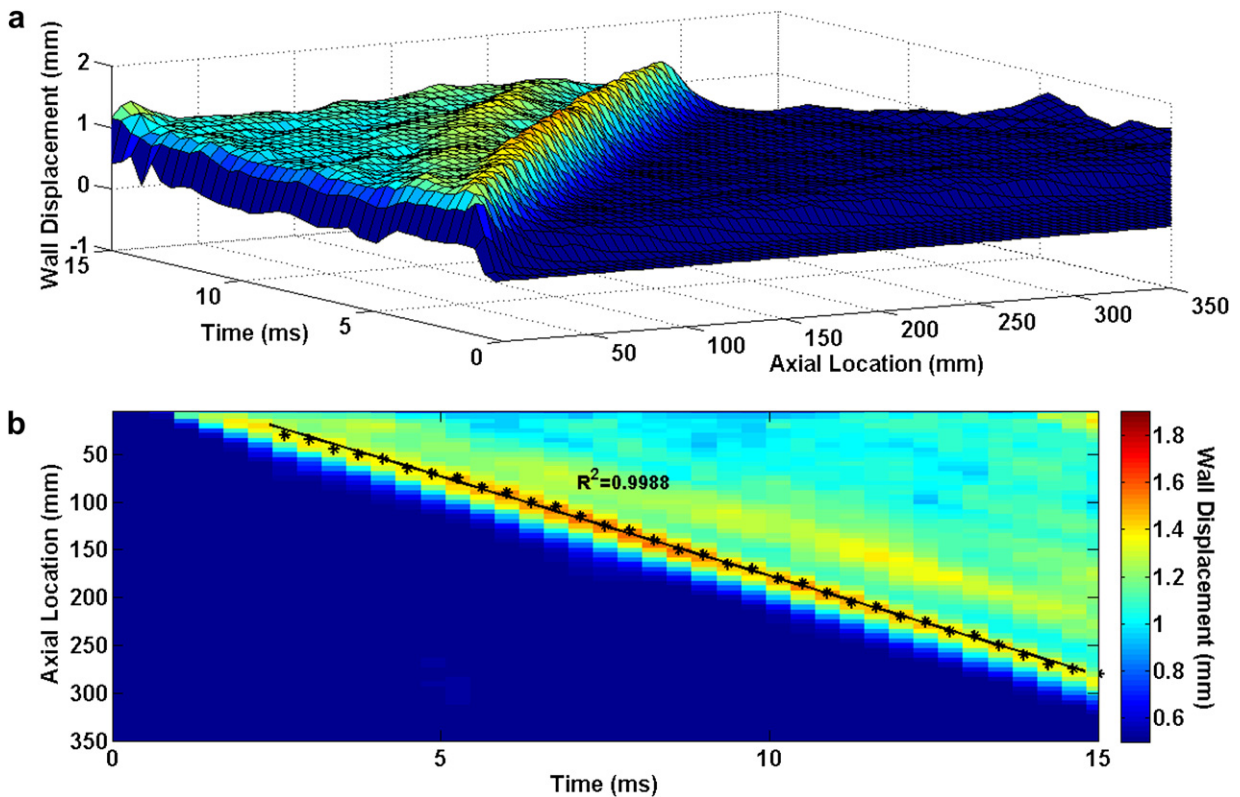


Figure 5 Homogenous model with Young's modulus of $E_5 = 7.68 \text{ MPa}$: (a) 3D waterfall plots of the wall displacement against temporal and spatial coordinates on the aortic wall. (b) 2D spatio-temporal plot of the wall displacement. Also shown are the peaks on the forward wave.

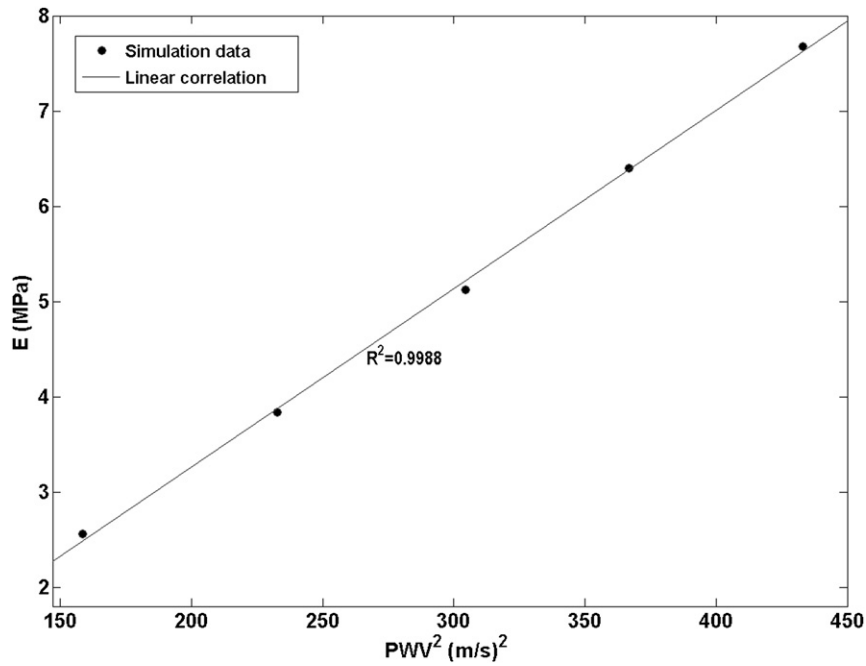


Figure 6 Linear correlation established ($R^2 = 0.9988$) between the pulse wave velocity-squared vs. Young's modulus data points obtained from five models with homogenous walls with a modulus of E_1 through E_5 .

displacement occurred at the site of the inclusion where the wall was the softest. The qualitative observation on the spatio-temporal plots shows the existence of a standing wave at the inclusion site. It is found that, similar to the hard inclusion model, the soft inclusion does not cause any

noticeable effect on the velocity of the forward wave. Based on the quantitative pulse wave velocity measurements obtained from the linear fits, the supra- and infra-inclusion PWVs are 20.32 m/s ($R^2 = 0.9951$) and 20.70 m/s ($R^2 = 0.9984$), respectively.

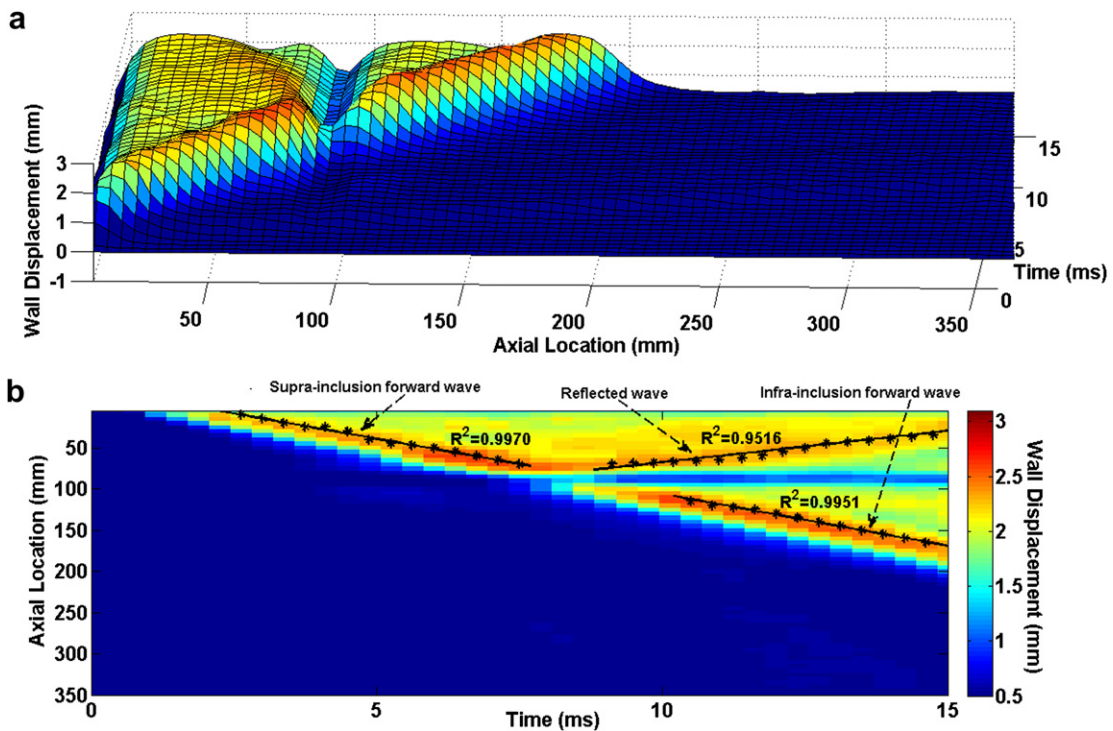


Figure 7 $E_1 = 2.56 \text{ MPa}$ arterial wall with $E_{hard-incl} = 7.68 \text{ MPa}$ hard inclusion: (a) 3D waterfall plots of the wall displacement against temporal and spatial coordinates on the aortic wall. (b) 2D spatio-temporal plot of the wall displacement. Also shown are the peaks on the forward and reflected waves.

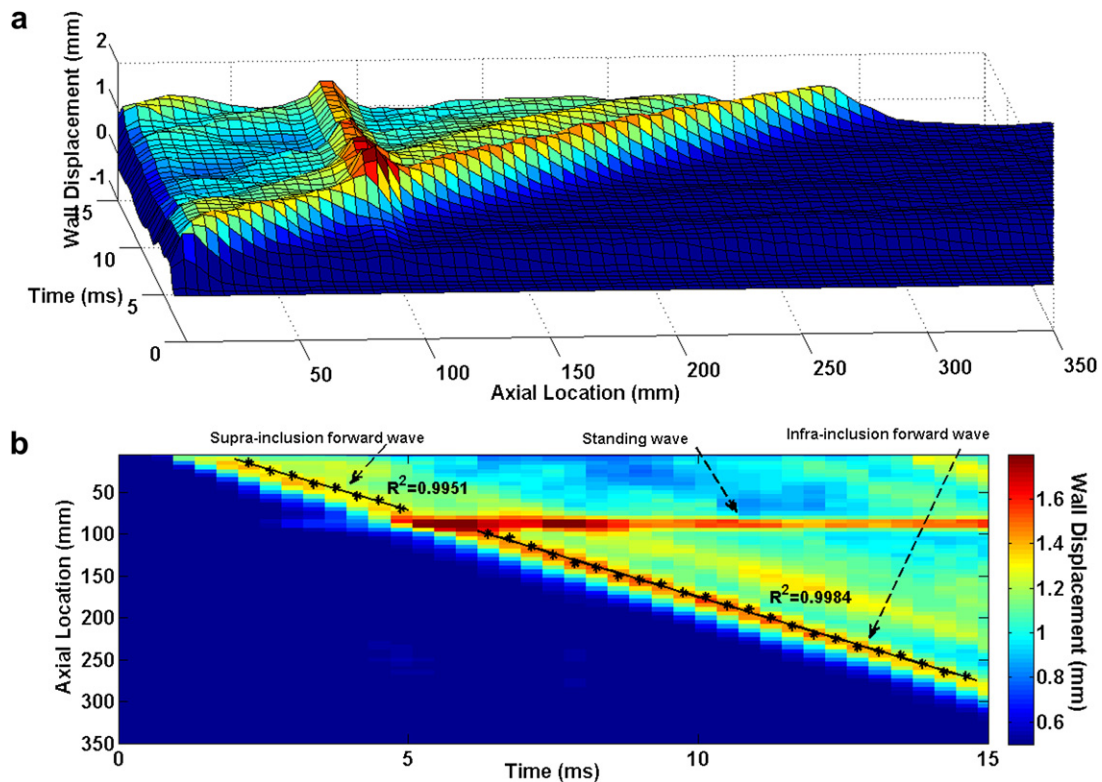


Figure 8 $E_5 = 7.65$ MPa arterial wall with $E_{soft-incl} = 2.56$ MPa soft inclusion: (a) 3D waterfall plots of the wall displacement against temporal and spatial coordinates on the aortic wall. (b) 2D spatio-temporal plot of the wall displacement. Also shown are the peaks on the forward waves.

Discussion

The current gold standard of noninvasive estimation of PWV in clinical practice is to obtain a global measure by determining the temporal pulse pressure profiles in two remote sites, typically the carotid and femoral arteries.^{16,26} However, the carotid-femoral method suffers from major issues such as the lack of knowledge of the exact arterial geometry and the assumption of a single longitudinal flow direction which can impair the accuracy of the method by underestimating/overestimating the true traveled distance. Yet, the most important disadvantage of the method could be the global nature of the measurement which averages the PWV over a long distance.³⁵ The disadvantage of global PWV measurements is previously discussed considering that the majority of the vascular diseases induce focal changes.^{32–34}

This study reports the use of numerical FSI modeling of the aortic pulse wave propagation in order to shed light into the effects of regional stiffness changes on the global PWV measures. Five homogenous models of increasing stiffness as well as two models with hard and soft inclusions were examined.

Supplementary videos of the animated results can be found at [doi:10.1016/j.artres.2012.05.004](https://doi.org/10.1016/j.artres.2012.05.004).

The results from the homogenous models showed that the numerical model developed was able to effectively capture the correlation between the increasing wall

modulus and the PWV^2 as established by the high correlation coefficient of $R^2 = 0.9988$ (Fig. 6).

Qualitative examination of the PWI spatio-temporal plots obtained from the inclusion models could be used to identify the existence and nature of the inclusions. Figs. 3 and 7 show the PWI spatio-temporal maps of the wall motion at 2.56 MPa without and with the hard inclusion of 7.68 MPa, respectively. As seen in Fig. 7, the hard inclusion caused a reflection wave which was not seen on the homogenous model (Fig. 3). In the case of the soft inclusion, Figs. 5 and 8 show the spatio-temporal maps of the wall motion at 7.68 MPa without and with the soft inclusion of 2.56 MPa, respectively. Unlike in the case of the homogenous model (Fig. 5), Fig. 8 showed the soft inclusion generating a standing wave at the inclusion site. The emergence of the reflected and standing waves can be used as potential markers to identify the regional increase and decrease in the wall stiffness, respectively. Additionally, the part of the spatio-temporal plots associated with the displacement of the inclusion showed up as a region of minimum (maximum) displacement on the site of the hard (soft) inclusion, respectively (Figs. 7 and 8), while the width of that region appears to be dependent on the inclusion size. Further quantification of such a relationship is needed in estimating not only the regional stiffness change but also the size of the lesion based on PWI *in vivo*.

Table 1 summarizes the PWVs obtained from the model with different parameters. The results show that a regional change in the wall stiffness, whether softening or

Table 1 Summary of the PWV measurements on models with homogenous and inhomogeneous (inclusion) models.

Model	Young's modulus (MPa)	Wave type	PWV (m/s)
Homogenous	Wall: 2.56	Forward	12.59
	Wall: 3.84	Forward	15.25
	Wall: 5.12	Forward	17.45
	Wall: 6.40	Forward	19.15
	Wall: 7.68	Forward	20.81
Hard inclusion	Wall: 2.56 / Inclusion: 7.68	Supra-inclusion forward	12.24
		Reflected	7.61
		Infra-inclusion forward	12.59
Soft inclusion	Wall: 7.68 / Inclusion: 2.56	Supra-inclusion forward	20.32
		Reflected	0 (<i>i.e. standing</i>)
		Infra-inclusion forward	20.70

stiffening, may not induce measurable effects on the downstream PWV. In the case of the hard inclusion, the supra-inclusion PWV differed from that of the homogenous model by only -2.78% where the infra-inclusion PWV did not show any measurable difference. Similarly, in the case of the soft inclusion, the supra- and infra-inclusion PWVs had only a -2.35% and 0.53% difference from the true PWV in the homogeneous model, respectively. This observation indicates that even high regional stiffness contrasts are not detectable by global PWV measurements. In addition, the PWV measured on the reflected wave was about 40% lower than that measured on the forward wave using the same model parameters. This could likely be due to the relative proximity of the inclusion site to the ends of the cylinder (*i.e.* at 90 mm distance from the tube inlet), which causes the reflected wave to be attenuated immediately after its formation and not freely propagating. Ongoing parametric studies are carried out to quantify the effects of vessel length and inclusion properties such as inclusion size, inclusion modulus contrast, and location of (multiple) inclusion(s) on the wave propagation pattern. The results from these studies would provide a better and more quantitative understanding of the wave propagation along an inhomogeneous wall.

Given the near incompressibility of the tissue, an increase in r (radius) during pulsation could be accompanied by a decrease in t (thickness), and therefore the r/t ratio could also be a variable during the Moens–Korteweg-based estimation of the E on the inclusion models. It was found that there could be a difference in the r/t ratio around 5–15%, depending on the inclusion modulus contrast, which is negligible compared to the 150–300% change in E .

Finite-element simulations for describing such dynamic phenomena could serve as a powerful tool but could also be compromised by a number of factors. First, the

computational cost can potentially be an impediment particularly in the case of full 3D patient specific complex geometries. This may require focal mesh density enhancements and computations over multiple cardiac cycles in order to achieve steady state behavior of wall regional motion. In the present study, however, the computational cost was relatively low owing largely to the simple straight-tube geometry and the simulation period of a single pulsatile cycle. Second, the solution of the simulation models was significantly affected by the initial and boundary conditions – neither of which can ideally mimic the *in vivo* state – and should be interpreted carefully in the context of the application. An isolated cylindrical tube with a linearly elastic wall being stimulated by an impulse fluid velocity would be in best agreement with the Moens–Korteweg formulation. In particular, the perfect symmetry of the solid and fluid geometries, initial and boundary conditions, fluid–solid interface, etc., ensure the formation and free propagation of a symmetric wave while the tube cross-section remains circular and inplane throughout.

The results presented here may not be representative of the *in vivo* configurations. However, this constitutes the first time –to the best of our knowledge– that the effects of inclusion on wave propagation were studied and the shortcoming of the global PWV measurements on detecting the local changes in the stiffness was observed. The present results on the straight-geometry provide good insight on how to assess and interpret the regional variations obtained from PWI *in vitro* and *in vivo* where the complexities of a more inhomogeneous wall, irregular geometry and physiological conditions may occur simultaneously. Ongoing studies are being conducted to adapt physiological conditions to the model such as a patient-specific blood velocity profile using Doppler ultrasound.

Conclusion

The present study primarily aimed at showing the feasibility of using the numerical methods to simulate the pulse wave propagation in simple aorta models and compute the local Pulse Wave Velocity (PWV) to detect changes in regional stiffness. The results indicated the significance of using Pulse Wave Imaging (PWI), over traditional methods such as carotid-femoral PWV measurement, in accurately depicting the change in arterial stiffness where global PWV fails. A finite-element model of fluid-structure interaction in straight-geometry arteries with homogenous and inhomogeneous walls were established to perform PWI *in silico*. The spatio-temporal map of the wall deformation obtained from the PWI enables the depiction of the inclusion and its size. It also provides important information on the regional propagation of the forward, reflected and standing waves which could be used for better identification of the regional wall discontinuities. Most importantly, similar PWVs were found for the waves upstream and downstream of the inclusion –with neither of them significantly different from the PWV on the homogenous model– emphasizing thus that the methods based on global PWV measurements may not be suited for detecting small, regional changes in the wall stiffness as encountered under pathological conditions. The

outcome of this study encourages the potential application of PWI for the noninvasive estimation of regional changes in arterial PWV and wall stiffness—an important biomarker for a wide range of cardiovascular-related diseases and treatment thereof. Future studies are needed to further implement the method on patient-specific and physiological aorta models.

Acknowledgements

This study was supported in part by the National Institutes of Health (R01-HL098830).

Appendix A. Supplementary data

Supplementary data related to this article can be found online at doi:10.1016/j.artres.2012.05.004.

References

- Safar M. Pulse pressure in essential hypertension: clinical and therapeutical implications. *J Hypertens* 1989;7:769–76.
- Laurent S, Katsahian S, Fassot C, Tropeano A, Gautier I, Laloux B, et al. Aortic stiffness is an independent predictor of fatal stroke in essential hypertension. *Stroke* 2003;34:1203–6.
- Boutouyrie P, Tropeano A, Asmar R, Gautier I, Benetos A, Lacolley P, et al. Aortic stiffness is an independent predictor of primary coronary events in hypertensive patients: a longitudinal study. *Hypertension* 2002;39:10–5.
- Woodman R, Watts G. Measurement and application of arterial stiffness in clinical research: focus on new methodologies and diabetes mellitus. *Med Sci Monit* 2003;9:RA81–9.
- Mahfouz Badran H, Elnoamany M. Impact of type 2 diabetes mellitus on aortic elastic properties in normotensive diabetes: Doppler tissue imaging study. *J Am Soc Echocardiogr* 2006;19:1471–81.
- Verbeke F, Vanholder R, Rensma PL, Wikstrom B, Jensen PB, Krzesinski J-M, et al. Role of aortic calcification, stiffness and wave reflections in cardiovascular risk in dialysis patients: baseline data from the CORD study. *Artery Res* 2010;4:81–90.
- Blacher J, Guerin AP, Pannier B, Marchais SJ, London GM. Arterial calcifications, arterial stiffness, and cardiovascular risk in end-stage renal disease. *Hypertension* 2001;38:938–42.
- He C, Roach MR. The composition and mechanical properties of abdominal aortic aneurysms. *J Vasc Surg* 1994;20:6–13.
- Marque V, Kieffer P, Gayraud B, Lartaud-Idjouadiene I, Ramirez F, Atkinson J. Aortic wall mechanics and composition in a transgenic mouse model of Marfan syndrome. *Arterioscler Thromb Vasc Biol* 2001;21:1184–9.
- Xiong J, Wang S, Zhou W, Wu J. Measurement and analysis of ultimate mechanical properties, stress-strain curve fit, and elastic modulus formula of human abdominal aortic aneurysm and nonaneurysmal abdominal aorta. *Vascular Surgery* 2008;189–95.
- Inzoli F, Boschetti F, Zappa M, Longo T, Fumero R. Biomechanical factors in abdominal aortic aneurysm rupture. *Eur J Vasc Endovasc Surg* 1993;7.
- Fillinger MF, Raghavan ML, Marra SP, Cronenwett JL, Kennedy FE. *In vivo* analysis of mechanical wall stress and abdominal aortic aneurysm rupture risk. *J Vasc Surg* 2002;36:589–97.
- Choke E, Cockerill G, Wilson RW, Sayed S, Dawson J, Loftus IM, et al. A review of biological factors implicated in abdominal aortic aneurysm rupture. *Eur J Vasc Endovasc Surg* 2005;30:227–44.
- Fujikura K, Luo J, Gamarnik V, Pernot M, Fukumoto R, Tilson M, et al. A novel noninvasive technique for pulse-wave imaging and characterization of clinically-significant vascular mechanical properties *in vivo*. *Ultrason Imaging* 2007;29:137–54.
- Mancia G, De Backer G, Dominiczak A, Cifkova R, Fagard R, Germano G, et al. ESH-ESC practice guidelines for the management of arterial hypertension: ESH-ESC task Force on the Management of Arterial Hypertension. *J Hypertens* 2007:1751–62.
- Laurent S, Cockcroft J, Van Bortel L, Boutouyrie P, Giannattasio C, Hayoz D, et al. Expert consensus document on arterial stiffness: methodological issues and clinical applications. *Eur Heart J* 2006;27:2588–605.
- Nichols W, O'Rourke M. *McDonald's blood flow in arteries: theoretical, experimental and clinical principles*. London, UK: Hodder Arnold Publication; 2005.
- O'Rourke M, Staessen J, Vlachopoulos C, Duprez D, Plante G. Clinical applications of arterial stiffness; definitions and reference values. *Am J Hypertens* 2002;15:426–44.
- Moens A. *Die Pulskurve* 1878.
- Korteweg D. Über die Fortpflanzungsgeschwindigkeit des Schalles in Elastischen Rohren. *Ann Phys Chem* 1878;5:52–537.
- Olufsen M. Structured tree outflow condition for blood flow in larger systemic arteries. *Am J Physiol* 1999;276:H257–68.
- Kinsler LE, Frey AR, Coppens AB, Sanders JV. *Fundamentals of acoustics*. New York, NY: Wiley; 2000.
- Fung Y. *Biomechanics: circulation*. New York, NY: Springer-Verlag; 1997.
- O'Rourke M, Franklin S. Arterial stiffness: reflections on the arterial pulse. *Eur Heart J* 2006;27:2497–8.
- Mookerjee A, Al Jumaily A, Lowe A. Arterial pulse wave velocity measurement: different techniques, similar results—implications for medical devices. *Biomech Model Mechanobiol* 2010;9:773–81.
- Pannier B, Avolio A, Hoeks A, Mancia G, Takazawa K. Methods and devices for measuring arterial compliance in humans. *Am J Hypertens* 2002;15:743–53.
- Chiu Y, Shroff S. Determination of pulse velocities with computerised algorithms. *Am Heart J* 1991;121:1460–9.
- Davies J, Struthers A. Pulse wave analysis and pulse wave velocity: a critical review of their strengths and weaknesses. *Hypertension* 2003;21:463–72.
- Millasseau SC, Stewart AD, Patel SJ, Redwood SR, Chowienczyk PJ. Evaluation of carotid-femoral pulse wave velocity: influence of timing algorithm and heart rate. *Hypertension* 2005;45:222–6.
- Lantelme P, Mestre C, Lievre M, Gressard A, Milon H. Heart rate: an important cofounder of pulse wave velocity assessment. *Hypertension* 2002;39:1083–7.
- Vappou J, Luo J, Konofagou E. Pulse wave imaging for noninvasive and quantitative measurement of arterial stiffness *in vivo*. *Am J Hypertens* 2010;23:393–8.
- Choke E, Cockerill G, Dawson J, Wilson RW, Jones A, Loftus IM, et al. Increased Angiogenesis at the site of abdominal aortic aneurysm rupture. *Ann NY Acad Sci* 2006;1085:315–9.
- Vande Geest JP, Schmidt DE, Sacks MS, Vorp DA. The effects of Anisotropy on the stress analyses of patient-specific abdominal aortic aneurysms. *Ann Biomed Eng* 2008;36:921–32.
- Palmieri D, Pane B, Barisione C, Spinella G, Garibaldi S, Ghigliotti G, et al. Resveratrol counteracts systemic and local inflammation involved in early abdominal aortic aneurysm development. *Surg Res* 2011;171:237–46.
- Segers P, Kips J, Trachet B, Swillens A, Vermeersch S, Mahieu D, et al. Limitations and pitfalls of non-invasive measurement of arterial pressure wave reflections and pulse wave velocity. *Artery Res* 2009;1:79–88.

36. Brands P, Willigers J, Ledoux L, Reneman R, Hoeks A. A noninvasive method to estimate pulse wave velocity in arteries locally by means of ultrasound. *Ultrasound Med Biol* 1998;24:1325–35.
37. Meinders J, Kornet L, Brands P, Hoeks A. Assessment of local pulse wave velocity in arteries using 2D distension waveforms. *Ultrasound Imaging* 2001;23:199–215.
38. Rabben S, Stergiopoulos N, Hellevik L, Smiseth O, Slordahl S, Urheim S, et al. Ultrasound-based method for determining pulse wave velocity in superficial arteries. *Biomechanics* 2004;37:1615–22.
39. Eriksson A, Greiff E, Loupas T, Persson M, Pesque P. Arterial pulse wave velocity with tissue Doppler imaging. *Ultrasound Med Biol* 2002;28:571–80.
40. Hermeling E, Reesink K, Reneman R, Hoeks A. Measurement of local pulse wave velocity: effects of signal processing on precision. *Ultrasound Med Biol* 2007;33:774–81.
41. Hoctor R, Dentinger A, Thomenius K. Array signal processing for local arterial pulse wave velocity measurement using ultrasound. *IEEE Trans Ultrason Ferroelectr Freq Control* 2007;54:1018–27.
42. Benthin M, Dahl P, Ruzicka R, Lindstrom K. Calculation of pulse-wave velocity using cross-correlation - Effects of reflexes in the arterial tree. *Ultrasound Med Biol* 1991;17:461–9.
43. Hartley C, Taffet G, Michael L, Pham T, Entman M. Noninvasive determination of pulse-wave velocity in mice. *Am J Physiol Heart Circ Physiol* 1997;42:H494–500.
44. Williams R, Needles A, Cherin E, Zhou Y, Henkelman R, Adamson S, et al. Noninvasive ultrasonic measurement of regional and local pulse-wave velocity in mice. *Ultrasound Med Biol* 2007;33:1368–75.
45. Couade M, Pernot M, Messas E, Emmerich J, Hagège A, Fink M, et al. Ultrafast imaging of the arterial pulse wave. *IRBM* 2011;32:106–8.
46. Bolster B, Atalar E, Hardy C, McVeigh E. Accuracy of arterial pulse-wave velocity measurement using MR. *Magn Reson Imaging* 1998;8:878–88.
47. Boese J, Bock M, Schoenberg S, Schad L. Estimation of aortic compliance using magnetic resonance pulse wave velocity measurement. *Phys Med Biol* 2000;45:1703–13.
48. Macgowan C, Henkelman R, Wood M. Pulse-wave velocity measured in one heartbeat using MR tagging. *Magn Reson Med* 2002;48:115–21.
49. Shao X, Fei D, Kraft K. Computer-assisted evaluation of aortic stiffness using data acquired via magnetic resonance. *Comput Med Imaging Graph* 2004;28:353–61.
50. Yu H, Peng H, Wang J, Wen C, Tseng W. Quantification of the pulse wave velocity of the descending aorta using axial velocity profiles from phase-contrast magnetic resonance imaging. *Magn Reson Med* 2006;56:876–83.
51. Luo J, Fujikura K, Tyrie L, Tilson M, Konofagou E. Pulse wave imaging of normal and aneurysmal abdominal aortas *in vivo*. *IEEE Transactions Medical Imaging* 2009;28:477–86.
52. Luo J, Lee W-N, Wang S, Konofagou E. Pulse wave imaging of human abdominal aortas *in vivo*. *Proc IEEE Ultrason Symp* 2008;2008:859–62.
53. Wang S, Lee W-N, Provost J, Luo J, Konofagou EA. Composite high-frame-rate system for clinical cardiovascular imaging. *IEEE Trans Ultrasonics Ferroelectrics Frequency Control* 2008;55:2221–33.
54. Vappou J, Luo J, Konofagou E. *Regional measurement of arterial stiffness using Pulse Wave Imaging: Phantom validation and preliminary clinical results*. Proc of IEEE Ultrasonics Symp 2010.
55. Li R, Luo J, Balaran S, Chaudhry F, Lantis J, Shahmirzadi D, et al. *In-vivo application of pulse wave imaging for arterial stiffness measurement under normal and pathological conditions*. 33rd Annual International IEEE EMBS Conference, Boston, MA 2011.
56. Vappou J, Luo J, Okajima K, Tullio M, Konofagou E. Aortic pulse wave velocity measured by pulse wave imaging (PWI): a comparison with applanation tonometry. *Artery Res* 2011;5:65–71.
57. Leung JH, Wright AR, Cheshire N, Crane J, Thom SA, Hughes AD, et al. Fluid structure interaction of patient specific abdominal aortic aneurysms: a comparison with solid stress models. *Biomed Eng Online* 2006;5:33.
58. Simon BR, Kaufmann MV, McAfee MA, Baldwin AL. Finite element models for arterial wall mechanics. *J Biomech Eng* 1993;115:489–96.
59. Rissland P, Alemu Y, Einav S, Ricotta J, Bluestein D. Abdominal aortic aneurysm risk of rupture: patient-specific FSI simulations using anisotropic model. *ASME J Biomech Eng* 2009;131:031001.
60. Ayyalasomayajula A, Vande Geest J, Simon B. Porohyperelastic finite element modeling of abdominal aortic aneurysms. *J Biomech Eng* 2010;132:104502.
61. Zheng J, Abendschein DR, Okamoto RJ, Yang D, McCommis KS, Misselwitz B, et al. MRI-based biomechanical imaging: initial study on early plaque progression and vessel remodeling. *Magn Reson Imaging* 2009;27:1309–18.
62. Ivankovic A, Karac A, Dendrinis E, Parker K. Towards early diagnosis of atherosclerosis: the finite volume method for fluid-structure interaction. *Biorheology* 2002;39:401–7.
63. Kelly SC, O'Rourke MJA. Two-system, single-analysis, fluid-structure interaction technique for modelling abdominal aortic aneurysms. *Proc Inst Mech Eng H* 2011;224:955–69.
64. Pelerin JL, Kulik C, Goksu C, Coatrieux JL, Rochette M. Fluid/structure interaction applied to the simulation of Abdominal Aortic Aneurysms. *Conf Proc IEEE Eng Med Biol Soc* 2006;1:1754–7.
65. Scotti CM, Jimenez J, Muluk SC, Finol EA. Wall stress and flow dynamics in abdominal aortic aneurysms: finite element analysis vs. fluid-structure interaction. *Comput Methods Biomech Biomed Engin* 2008;11:301–22.
66. Vappou J, Zervantonakis I, Luo J, Konofagou EE. Finite element modeling of the pulse wave propagation in the aorta for simulation of the pulse wave imaging (PWI) method. *Computational Biomech Med* 2008;118–27 (MICCAI 2008 Workshop).
67. Shahmirzadi D, Li R, Konofagou E. *Aortic stiffness estimation via pulse wave imaging in patient-specific simulated and silicone phantom*. Hartford, CT: Biomedical Engineering Society Annual Meeting; 2011.
68. Shahmirzadi D, Li R, Konofagou E. *Simulated Pulse Wave Imaging for Local Stiffness Estimation of Patient-Specific Aorta*. Int Tissue Elasticity Conference, Arlington, TX 2011.
69. Shahmirzadi D, Li R, Konofagou EE. FSI modeling of aortic pulse wave propagation for stiffness estimation with validation against phantom and *in vitro* studies. *Biomech Eng*, 2012, in press.
70. Humphrey J. *Cardiovascular solid mechanics: cells, tissues, and organs*. New York: Springer-Verlag; 2002.
71. Kanyanta V, Ivankovic A, Karac A. Validation of a fluid-structure interaction numerical model for predicting flow transients in arteries. *J Biomech* 2009;42:1705–12.
72. Lide D. *CRC Handbook of chemistry and physics*. 70th Edn. 1990.
73. Kaatz U. Fundamentals of microwaves. *Radiat Phys Chem* 1995;45:539–48.